

Simulation of drop impact on substrate with micro-wells

Cite as: Phys. Fluids **34**, 062108 (2022); <https://doi.org/10.1063/5.0093826>

Submitted: 30 March 2022 • Accepted: 26 May 2022 • Accepted Manuscript Online: 27 May 2022 •
Published Online: 09 June 2022

 Ahmed Islam, Mark Sussman,  Hui Hu, et al.



View Online



Export Citation



CrossMark

ARTICLES YOU MAY BE INTERESTED IN

[Contact time of a droplet impacting hydrophobic surfaces](#)

Phys. Fluids **34**, 067104 (2022); <https://doi.org/10.1063/5.0092707>

[Dynamics of droplet impact on a superhydrophobic disk](#)

Phys. Fluids **34**, 062104 (2022); <https://doi.org/10.1063/5.0091277>

[Interface evolution characteristics of dual droplet successive oblique impact on liquid film](#)

Phys. Fluids **34**, 062115 (2022); <https://doi.org/10.1063/5.0096585>

APL Machine Learning

Open, quality research for the networking communities

Now Open for Submissions

LEARN MORE



Simulation of drop impact on substrate with micro-wells

Cite as: Phys. Fluids **34**, 062108 (2022); doi: [10.1063/5.0093826](https://doi.org/10.1063/5.0093826)

Submitted: 30 March 2022 · Accepted: 26 May 2022 ·

Published Online: 9 June 2022




View Online



Export Citation



CrossMark

Ahmed Islam,¹  Mark Sussman,² Hui Hu,³  and Yongsheng Lian^{1,a)} 

AFFILIATIONS

¹Mechanical Engineering Department, University of Louisville, Louisville, Kentucky 40223, USA

²Mathematics Department, Florida State University, Tallahassee, Florida 32306, USA

³Department of Aerospace Engineering, Iowa State University, Ames, Iowa 50011, USA

^{a)}Author to whom correspondence should be addressed: y0lian05@louisville.edu

ABSTRACT

In this paper, we numerically investigate drop impact on a micro-well substrate to understand the phenomena of non-wettability. The simulation is carried out by solving three-dimensional incompressible Navier–Stokes equations using a density projection method and an adaptive grid refinement algorithm. A very sharp interface reconstruction algorithm, known as the moment-of-fluid method, is utilized to identify the multi-materials and multi-phases present in the computation domain. Our simulations predicted that a micro-well with a deep cavity can significantly reduce a solid–liquid contact in the event of drop impact. The results from the drop impact on the micro-well substrate are compared with results from drop impact on a flat substrate. Significant differences are observed between these two cases in terms of wetted area, spreading ratio, and kinetic energy. Our simulation shows that under the same conditions, a drop is more apt to jump from a micro-well substrate than from a flat surface, resulting in smaller wetted area and shorter contact time. Based on the simulation results, we draw a drop jumping region map. The micro-well substrate has a larger region than the flat surface substrate. Finally, we present a comparative analysis between a flat substrate and a substrate constructed with a dense array of micro-wells and, therefore, show that the array of micro-wells outperforms the smooth substrate with regard to non-wettability and drop wicking capability.

Published under an exclusive license by AIP Publishing. <https://doi.org/10.1063/5.0093826>

INTRODUCTION

Numerous studies have been done over decades to understand the liquid–solid interactions with different substrate properties and solid surface hydrophilicity. In many cases, surface hydrophobicity is very much sought after, because liquid repellent properties can become useful in reducing contact times of the liquid–solid interaction.¹ The complex dynamics of contact time, which is generally described as the duration of the droplet contact and, consequently, the spreading and retracting phases, depends on the surface–liquid interactions.² Many researchers have deemed the spreading phase after drop impact to be particularly most important,^{3–5} and others have pointed out the importance of the retraction phase immediately after the spreading phase.⁶ In some applications, it is desired to prolong the contact time such as inkjet printing,^{7,8} pesticide transferring on crops,^{9–11} and spray cooling.¹² In other cases, it is desired to reduce the contact time such as anti-corrosion and self-cleaning^{13–16} application, spray cooling,^{17–19} and deicing and anti-icing methods in aviation/aircraft industries.^{20–22}

In the nature, there are many materials that exhibit superhydrophobicity with advancing contact angles ranging between 150° and 160° (Refs. 23–26) and generally classified as features due to following: (1) lubricated films, such like epicuticular wax, providing a layer between the solid and liquid phases, (2) roughness that can effectively entrap air and provide a barrier or a type of an insulation medium, and finally, (3) secondary texture with superimposing morphological surfaces. Focusing on the roughness of substrates, an idea coined from the nature, researchers have shown that an excellent non-wetting property could be achieved by micro-structures that encapsulate air or, in general, have additional gas or liquid phases.^{27,28} The underneath air entrapment dictates if a droplet would undergo the Cassie state that demonstrates partial wetting or non-wetting or Wenzel states that show complete wetting due to the liquid contacting the substrate while displacing the cushioning air.²⁹ Researchers focusing on fabricating superhydrophobic surfaces typically modify the surface property to provide certain degrees of roughness and use methods like abrasive polishing, plasma nano-texturing, etching, lithography, nano-coating and grit roughening, 3D printing, etc.^{30–35} All these certain

methods allow researchers to entrap air within the micro- and nano-structures by roughening the surface, such that the droplets can exhibit a Cassie–Baxter state of non-wettability instead of the Wenzel state of fully wettability as shown in Fig. 1. Micro- and macro-structures of many different kinds were researched in the past; such substrates feature triangular ridges,³⁶ small spherical feature,^{37–39} different types of fabrics,^{40,41} short conical structure,⁴² different sizes of half spheres,³⁸ large tubes,⁴³ and curved surfaces,⁴⁴ but most importantly, micro-pillars or micro-posts^{2,45–54} that enhance faster wicking or pancake bouncing are of great interest. Anisotropically wetting substrates, such stripes with chemically alternating hydrophilic and hydrophobic properties, are also sometimes considered more benefitting than isotropic substrates, like micro-pillars or micro-posts.⁵⁵

While the air pocket entrapment or encapsulation needed for superhydrophobic surfaces is thoroughly understood and widely recognized by the scientific community, most of the studies have continued to focus on the drop shape evolution, the aspect of velocity and pressure changes within the drop or the volume of liquid, and possible reductions in contact times. It is conveniently understood that all superhydrophobic surfaces are textured or rough surfaces that entrap air pockets,^{52,56–62} and droplets impacting on rough surfaces exhibit quick non-wetting and reduced contact times.⁶³ Similarly, with increased superhydrophobicity of rough surfaces, bulk kinetic energy (KE) is spent on spreading and retraction and less into useful transformational energy harnessed for out of plane jumping and, therefore, may lead to splashing and/or drop breakups into smaller satellite droplets.^{64,65} A very effective water repellency has been observed by Shen *et al.*²⁰ due to the rough surface where the water droplet bounced off before freezing, resulting in reduction in the icing strength because of low efficiency in thermal conduction between the water droplet and the cold solid surface. Bird *et al.*^{1,66} discussed that with micro-textured surfaces, controlling the extent of contact time can essentially dictate the mass, momentum, and energy exchange, and therefore, it should be minimized. They experimented drop impacting on the macroscopic structure/ridge to make axisymmetric recoil resulting in minimum contact timing. It is also theoretically suggested that thin spread textures are indispensable to trap air that results in reduced contact time.^{1,67,68} Quan and Zhang⁶⁹ studied micro-pillars of different types and shapes, including triangular, square, crisscross, and spherical cylinders, with crisscross showing the best bouncing ability, and such ability is attributed to large capillary pressure and the ability of capturing air in the gaps compared to other types of pillar shapes. Other

researchers also discussed about the toroidal rim instability⁷⁰ and the development of rotational velocities within the rim, therefore resulting in partial or complete rebound, prompt, corona, or receding breakup of droplets recoiling on superhydrophobic substrates that can entrap air pockets.^{71,72}

In this paper, we numerically investigated liquid water drop impact on a micro-well substrate and demonstrated how air inside a micro-well can prevent a water drop from wetting the bottom of the substrate. The micro-well surface is structurally different than any other types of a rough substrate that are hydrophobic in nature. Since the micro-well structure does not let air to escape from its cavity and seals the opening of the structure as the liquid drop contacts the edge of the solid, it is, therefore, different from other types of water repellent substrates. Also through this study, using the same concept of a large micro-well, we would show that the reduced wettability of a single micro-well can be expanded into an array of smaller micro-wells. At first, we describe the numerical approach to the problem using the moment-of-fluid (MOF) algorithm, and then we present the setup for the problem and demonstrate our accuracy and mesh sensitivity used in this study. Second, we use a single micro-well and show that drop impact at various speeds and contact angles can both benefit from the reduced liquid–solid interaction and air acting as a barrier. Using the concept of a single micro-well, we further demonstrate drop impact cases on a substrate with arrays of micro-wells and discuss the non-wettability compared to a substrate with no roughness features.

NUMERICAL METHODS

For any incompressible flow with two phases of a multiphase flow system, we seek the Navier–Stokes equation given by the following equation:

$$\frac{\partial \mathbf{U}}{\partial t} + \nabla \cdot (\mathbf{U}\mathbf{U}) = \frac{1}{\rho}(-\nabla p + \nabla \cdot \boldsymbol{\tau} + F_{tension} + (H)\mathbf{g}), \quad (1)$$

where $\mathbf{U} = (u, v, w)$ is the velocity vector, t is the time, p is the pressure, $\boldsymbol{\tau}$ is the shear stress tensor, H is the Heaviside function indicating different materials, and \mathbf{g} is the gravitational acceleration vector. Due to the constraint of incompressibility of each fluid present in the domain, the continuity equation gives us

$$\nabla \cdot \mathbf{U} = 0. \quad (2)$$

The advection equation becomes

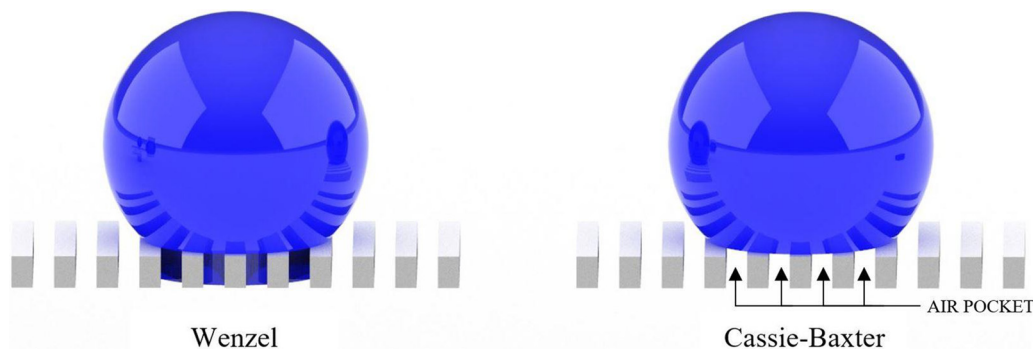


FIG. 1. Wenzel state (left) vs Cassie–Baxter state (right).

$$\frac{\partial H}{\partial t} + \mathbf{U} \cdot \nabla H = 0. \tag{3}$$

For multiple fluids present in a system, there should be a way to track each fluid. Let us consider two different fluids, designating the Heaviside function $H = 0$ for fluid 1 (e.g., air) and $H = 1$ for fluid 2 (e.g., water) to track the fluid in a volume. The Heaviside function in this case is defined as follows:

$$H_m(\mathbf{x}, t) = \begin{cases} 1 & \mathbf{x} \in \text{material } m, \\ 0 & \text{otherwise.} \end{cases} \tag{4}$$

Within the system, the volume averaged density for each phase is given as $\rho(\mathbf{H}) \equiv \sum_{m=1}^M \rho_m H_m$, and τ is the shear stress tensor defined as

$$\tau = \mu(\mathbf{H}) (\nabla \mathbf{U} + (\nabla \mathbf{U})^T). \tag{5}$$

Here, $\mu(\mathbf{H}) \equiv \sum_{m=1}^M \mu_m H_m$ is the viscosity, and the stress at the material interface will have the following jump condition due to the surface tension:

$$[(-pI + \tau) \cdot \mathbf{n}] = \sigma \kappa \mathbf{n}, \tag{6}$$

where σ is the surface tension coefficient and κ and \mathbf{n} are the curvature and unit normal of the interface, respectively.

For two-phase flow, the surface tension force term, $\mathbf{F}_{tension}$, between two materials is

$$\mathbf{F}_{tension} = \sigma_{1,2} (\nabla \cdot \mathbf{n}_m) \nabla H_m, \tag{7}$$

and the interface unit normal is

$$\mathbf{n}_m = \frac{\nabla H_m}{|\nabla H_m|}. \tag{8}$$

Moment-of-fluid interface reconstruction

A clear and visible separation and identification of the multiphases present with the domain is essential for each computational cell. The moment-of-fluid (MOF) method used in this paper has been developed in light of the generalized volume-of-fluid method (VOF), and the different phases are depicted by a plane in 3D or a line in 2D. This interface representation is known as a piecewise linear interface calculation (PLIC). For the moment-of-fluid (MOF) method, the material m distribution with its volume fraction in each computation cell is

$$F_{m,cell} = \frac{\Omega_{i,m}}{\Omega_{i,cell}} = \frac{1}{\Delta x \Delta y \Delta z} \int_{x_{i-1/2}}^{x_{i+1/2}} \int_{y_{j-1/2}}^{y_{j+1/2}} \int_{z_{k-1/2}}^{z_{k+1/2}} H_m(\mathbf{x}) dz dy dx, \tag{9}$$

where $\Omega_{i,cell}$ and $\Omega_{i,m}$ are the volume of cell $(i, j, \text{ and } k)$ and the volume of material m in the cell. The centroid of the material in the cell is

$$\mathbf{x}_m = \frac{\int_{x_{i-1/2}}^{x_{i+1/2}} \int_{y_{j-1/2}}^{y_{j+1/2}} \int_{z_{k-1/2}}^{z_{k+1/2}} \mathbf{x} H_m(\mathbf{x}) dz dy dx}{F_{m,cell}}. \tag{10}$$

In between the considered material regions, the interface between two materials can be represented as $\Gamma_{m1,m2}$ and \mathbf{n} as the unit normal vector always pointing away from the cell face, as shown in Fig. 2.

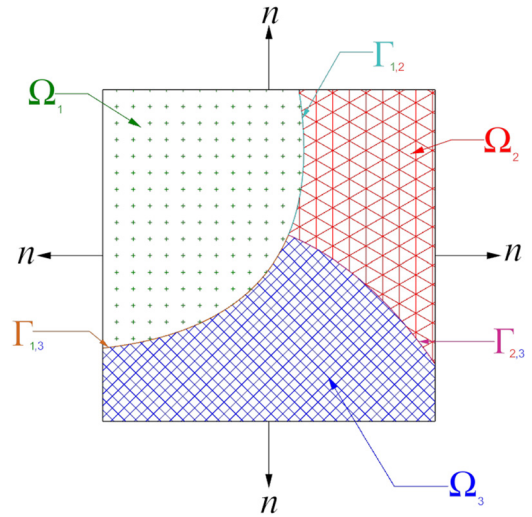


FIG. 2. Three materials with interface.

With the piecewise linear multi-material MOF reconstruction,⁷³ the interface in between two materials can be represented as a straight line with normal \mathbf{n} and intercept \mathbf{b} and stems from a reference volume, F_{ref} and reference centroid \mathbf{x}_{ref} . Therefore, the interface can be represented as

$$\Gamma = [x|\mathbf{n} \cdot (x - x_0) + b = 0]. \tag{11}$$

The normal for each of the cell representing more than one material can be written as follows:

$$\mathbf{n} = \begin{pmatrix} \sin(n) \cos(b) \\ \sin(n) \sin(b) \\ \cos(n) \end{pmatrix}. \tag{12}$$

As shown in Fig. 3, with the constrain set to match the actual volume to reference volume

$$|F_{reference,m}^c - F_{actual,m}^c(n, b)| = 0, \tag{13}$$

an error minimization criterion is employed with the following condition:

$$(n, b) = \text{argmin}(E_{MOF}) = \text{argmin} ||x_{reference} - x_{actual}(x, b)||. \tag{14}$$

With reference to Refs. 74–77, the Gauss–Newton algorithm tolerance for this equation provided by finding the slope is $\epsilon_{slope} = 10^{-10}$, and Brent’s method tolerance for finding the intercept is $\epsilon_{intercept} = 10^{-12}$. If the material within the computed cell is more than two types, a nested dissection algorithm is applied to perform the proper MOF reconstruction,⁷⁵ where the centroid for the subsequently reconstructed material is selected to be the farthest to the centroid of the un-captured volume. Further review on moment of the fluid reconstruction method can be found in other relevant literature works.^{73–75,77–83}

The following equations are used in the study to define different parameters and their non-dimensionalization characteristics: Weber number:

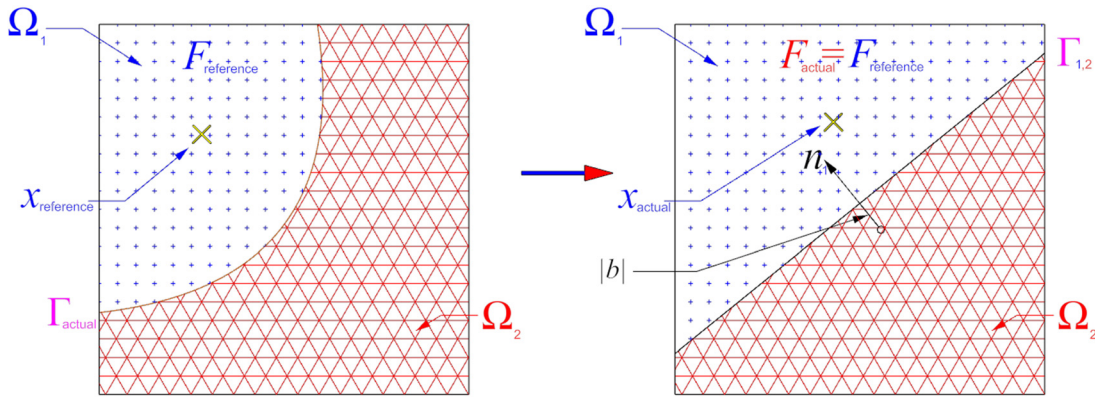


FIG. 3. MOF interface reconstruction.

$$We = \frac{\rho_l U_0^2 D_0}{\sigma}, \tag{15}$$

where ρ_l , U_0 , D_0 , and σ are the density of the liquid, the initial impact speed of the drop, the initial diameter of the drop, and the surface tension, respectively.

Time:

$$t^* = \frac{t}{\sqrt{\frac{\rho_l (0.5 D_0)^3}{\sigma}}}. \tag{16}$$

Spreading ratio:

$$\beta = \frac{D_{spread}}{D_0}. \tag{17}$$

Wetted area ratio:

$$A^* = \frac{A_{wetted}}{\pi \left(\frac{D_0}{2}\right)^2}, \tag{18}$$

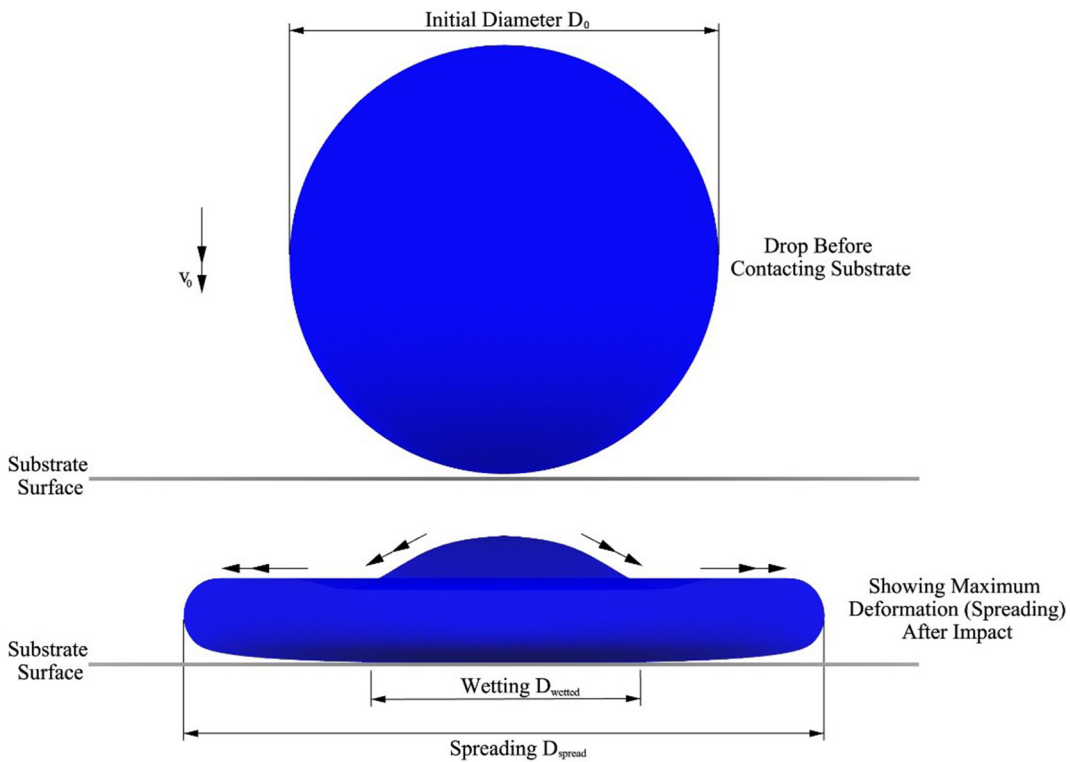


FIG. 4. Illustration of the drop initial, the spreading, and the wetting diameter after the event of impact on a surface.

where $A_{wetted} = \pi(\frac{D_{wetted}}{2})^2$ and the D_{wetted} is the diameter of the area of the liquid–solid contact (Fig. 4).

Kinetic energy in the z-direction (the direction of drop rebounding) is

$$KE^* = \frac{KE_z}{\rho_l \left(\frac{4}{3}\pi r_0\right)^3 U_0^2}, \tag{19}$$

where $r_0 = \left(\frac{D_0}{2}\right)$ and D_0 is defined earlier.

CODE VALIDATION

We first simulate a well-documented experimental study to show the capability of the numerical method. The experiment was conducted by Kim and Chun.⁸⁴ They studied a water drop impacting a flat substrate at a speed of 0.77 m/s. The radius of the water drop is 1.8 mm with a liquid density of 998 kg/m³ and a viscosity of 8.67 × 10⁻⁴ kg/ms. In the simulation, the dynamic contact angle model by Jiang *et al.*⁸⁵ is used

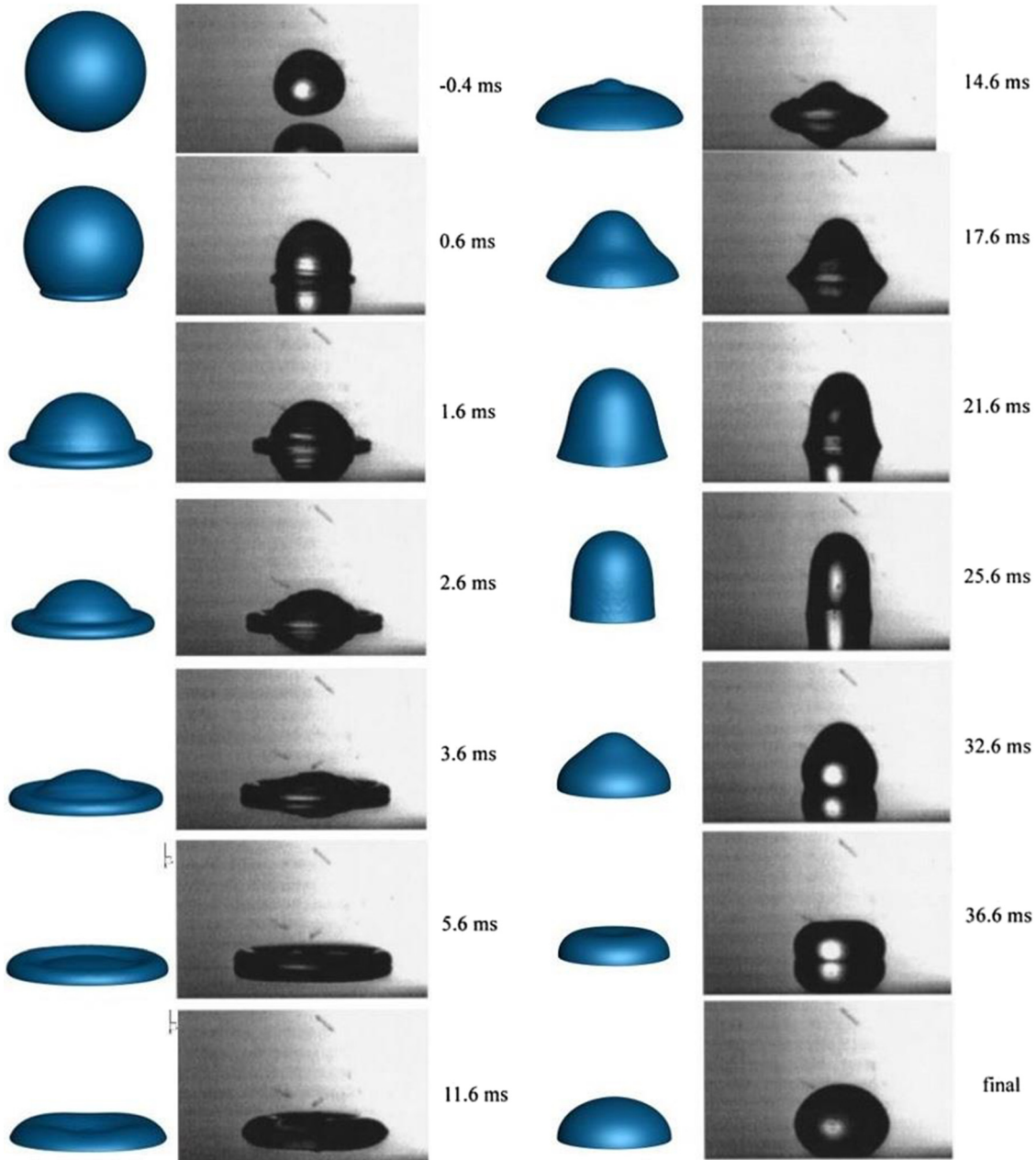


FIG. 5. Comparison between simulation (blue) and experiment (black) from Ref. 84.

$$\frac{\cos(\theta_e) - \cos(\theta_d)}{\cos(\theta_e) + 1} = \tanh(4.96Ca^{0.702}), \quad (20)$$

where θ_e , θ_a , and θ_r are the equilibrium, advancing, and receding contact angles and their values are 87.4° , 114° , and 52° , respectively. Ca is the capillary number defined as $Ca = \frac{\mu_l U_0}{\sigma}$, with μ_l being the viscosity of the liquid. The surface tensions between liquid and gas, liquid and solid, and solid and gas are 0.0728, 0.0695, and 0.0728 N/m, respectively. Figure 5 compares drop spreading and recoiling after impact between the experiment and simulation. A very fine mesh refinement of 40 cells per radius for the initial drop diameter coupled with the dynamic contact angle found to have an excellent match with the experimental maximum base diameter, and the time evolution of the adaptive mesh refinement (AMR) for drop spreading is shown in Fig. 6. A comparison of the non-dimensionalized base diameter

between the experiment and simulation is shown in Fig. 7. Agreement is also good. The code has been used to study other drop impact cases, and the results are reported by Yan *et al.*^{86,87}

RESULTS AND DISCUSSION

Drop impact on a single micro-well

The setup of drop impact on a single micro-well is shown in Fig. 8. The drop has a diameter of $250 \mu\text{m}$, and the micro-well has a diameter of $200 \mu\text{m}$ and a depth of $180 \mu\text{m}$. The equilibrium contact angle is 120° . A drop is initially positioned $1 \mu\text{m}$ above the micro-well with an initial velocity of 2 m/s. Table I shows the liquid and gas properties used. To show the pertinent features of the micro-well, we also simulate drop impact on a flat surface under the same conditions. The boundary conditions and the domain setup for the micro-well are shown in Fig. 9.

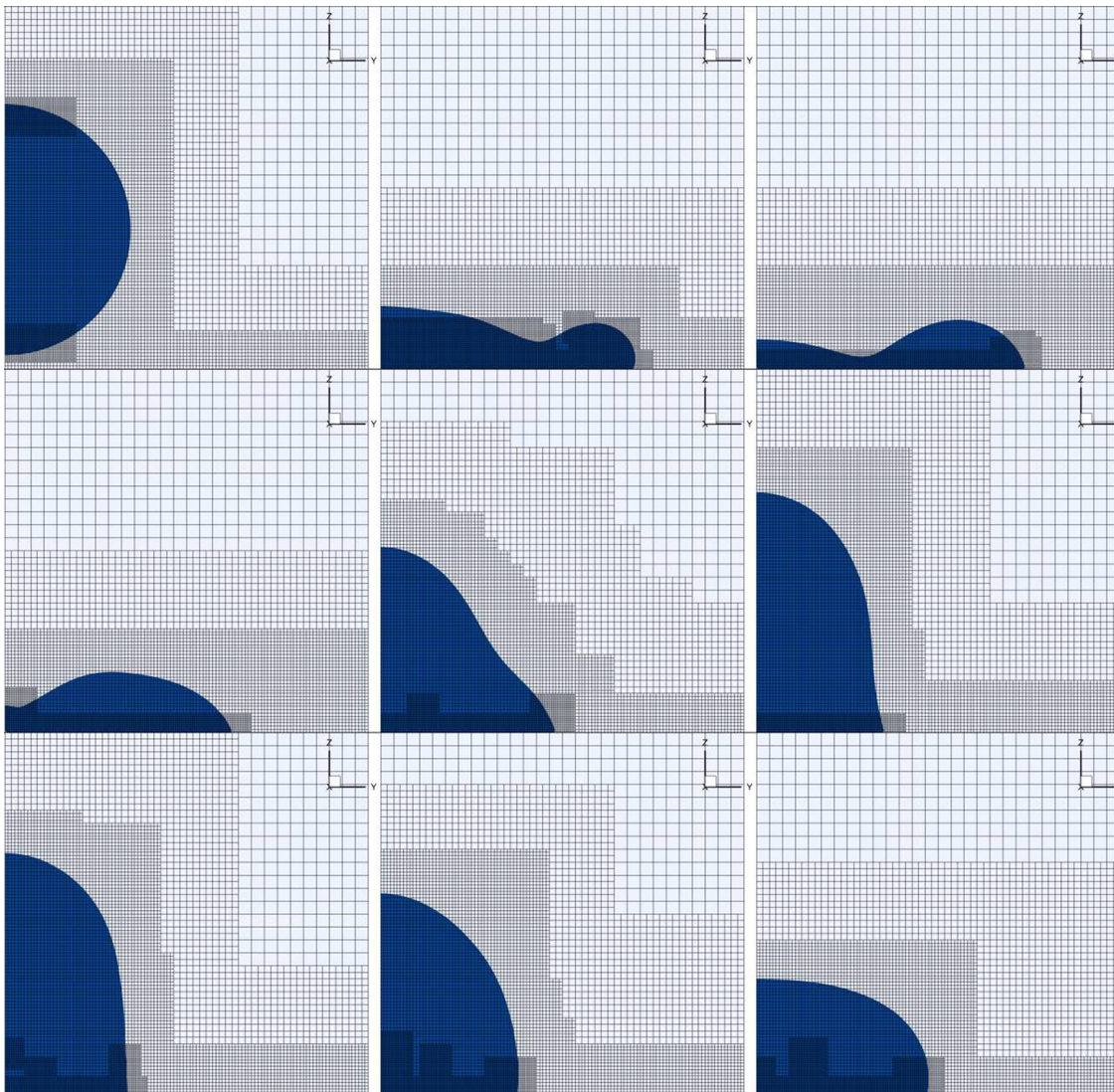


FIG. 6. Stepwise evolution of adaptive mesh refinement while the drop spreads and recedes.

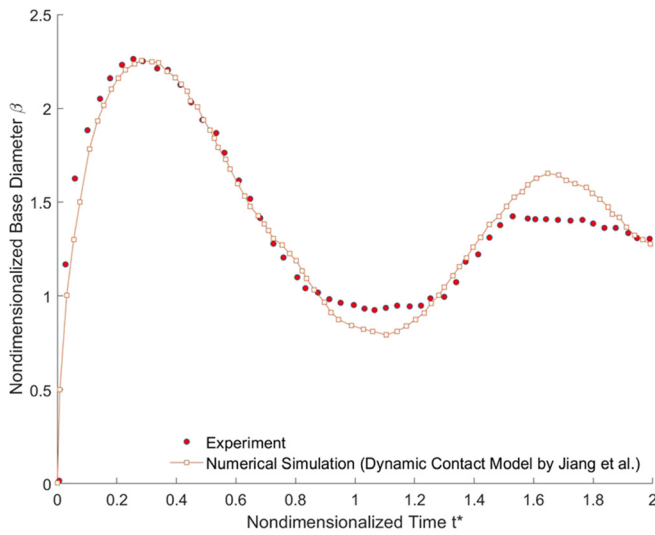


FIG. 7. Comparison of the non-dimensional base diameter between the experiment⁸⁴ and simulation. In the simulation, the dynamic contact angle model of Jiang *et al.*⁸⁵ is used.

Figure 10 shows the simulated drop spreading after impact on a flat substrate and a micro-well. In both cases, the drop spreads laterally but there is a noticeable difference between the two. As the bulk of drop enters the cavity of the micro-well, the drop remains suspended in the air without ever touching the well bottom, resulting in a much smaller wetted substrate in the case of the micro-well. Figure 11 shows the event of drop impacts for the two cases with the drop on the micro-well leaving much earlier than the drop on the flat substrate. The drop on the flat substrate eventually detaches from the surface much later than the flat substrate ($t = 0.7 \text{ ms}+$) but only to fall back and reattach to the surface within a very short period of time.

We use the spreading ratio and the wetted area ratio to explain the differences between the cases of two different surface types. The spreading ratio is the ratio of the maximum projected diameter of the

TABLE I. Liquid and gas properties.⁸⁸

	$\sigma \text{ (mN m}^{-1}\text{)}$	$\mu_l \text{ (mPa s)}$	$\mu_g \text{ (mPa s)}$	$\rho_l \text{ (kg m}^{-3}\text{)}$	$\rho_g \text{ (kg m}^{-3}\text{)}$
10 °C	72.7	1.308	0.02	999.7	1.25

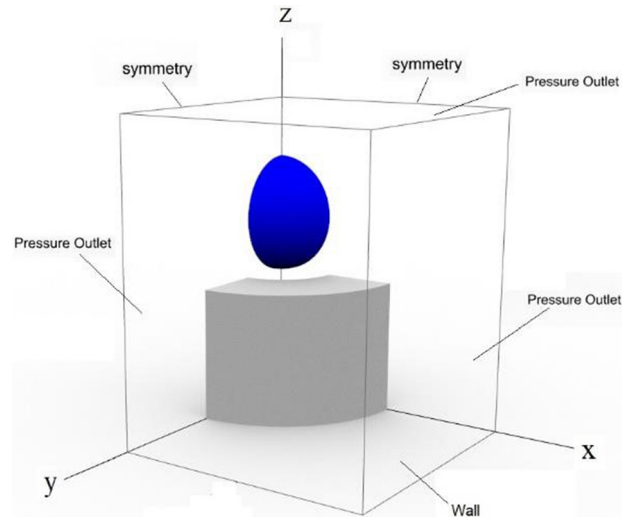


FIG 9. Domain setup and boundary conditions for the micro-well.

deformed drop to the diameter of the initially undeformed drop, as shown earlier in Fig. 4; the wetted area ratio denotes the ratio of the actual contact area between the solid and liquid phases over the projected area of the drop. The spreading ratio is defined in Eq. (17). The time variation against the spreading ratio is plotted in Fig. 12. The red line is the spreading ratio of the micro-well case, and the blue is the flat surface. Note that the drop takes longer to touch the micro-well surface than to touch the flat surface. As the drop closes the orifice of the micro-well, it remains suspended inside the cylindrical cavity, and

Drop impact on a single micro-well

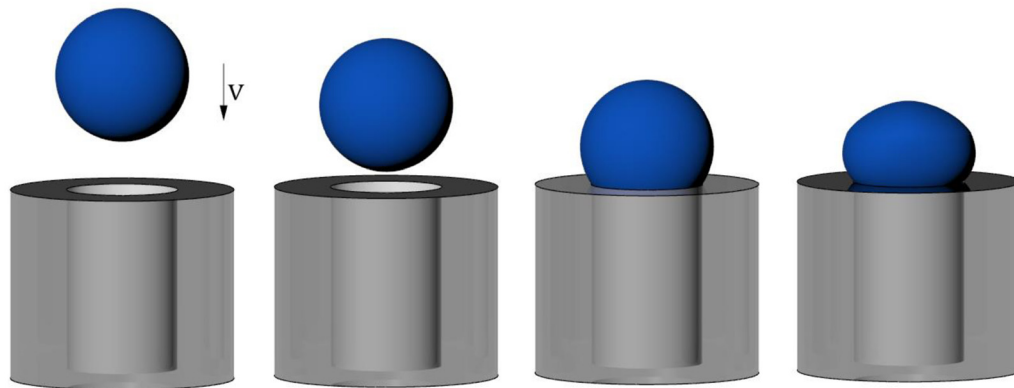


FIG. 8. Drop impact on a single micro-well shown as rendering.

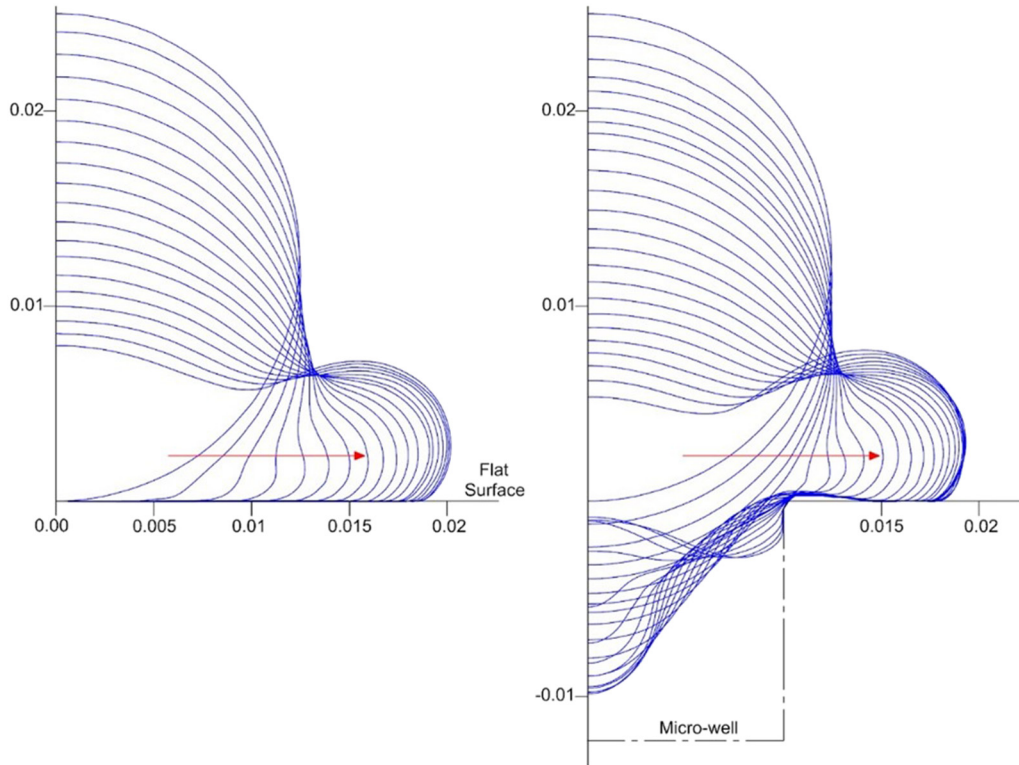


FIG. 10. Simulation of drop spreading on the flat surface (left) and the micro-well (right), only half of the x - y plane is shown here.

the entrapped air in the micro-well prevents the drop from wetting the bottom of the micro-well. The micro-well case has a smaller spreading ratio, hence a quicker drop retraction and jump off than the flat surface case. The jump off time for the micro-well is $t^* = 2.33$ and is $t^* = 4.76$ for the flat surface case. The drop on the flat substrate quickly returns (falls back) after a very short period of detachment, while on the micro-well, it departs much earlier and eventually achieves a higher trajectory.

To further illustrate the pertinent feature of drop impact on the micro-well, we present the wetting region, which represents the liquid-

substrate contact over time. When the drop impacts on the micro-well, it wets a small surface area in contrast to when it hits a flat surface. The wetting region is much different between the two cases, and therefore, we present the wetted area ratio along with previously presented spreading ratio comparison. While the spreading ratio showed the lateral distance traveled by the drop, the effective wetted area ratio is the actual contact area between the drop and substrate. The change in the wetted area over time is plotted in Fig. 13. The drop has a 47% less wetted area in the micro-well case than in the flat surface case. Also note that the drop departs from the micro-well substrate much

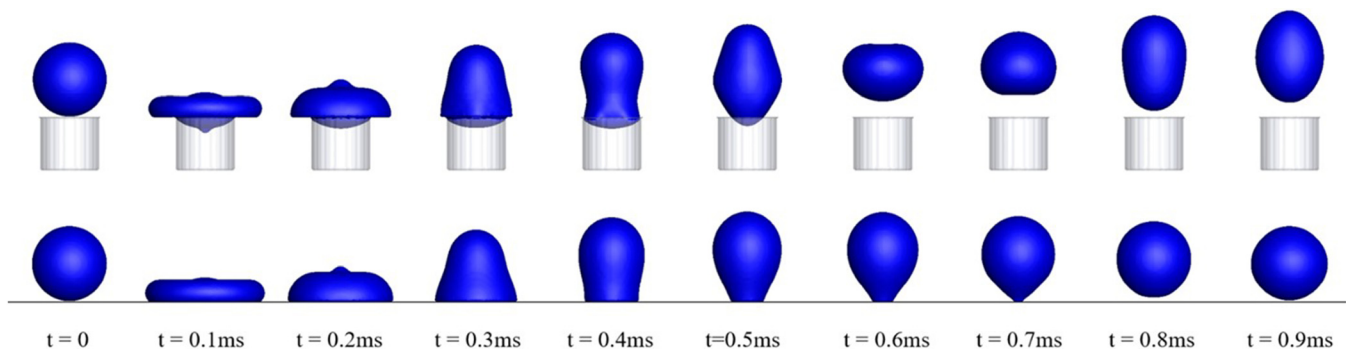


FIG. 11. Drop impact on a micro-well (top) vs flat (bottom): drop detaches and jumps away from the micro-well substrate, but detachment on the flat substrate is very slow and the drop quickly returns to the surface on the flat substrate.

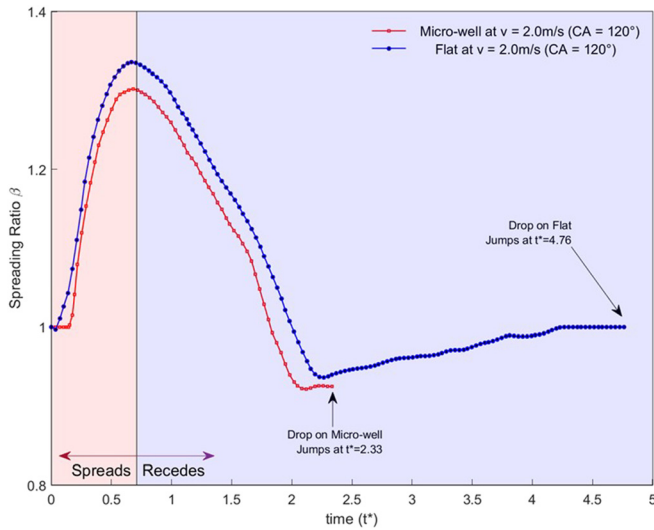


FIG. 12. Time variation of the spreading ratio of drop impacting on the flat substrate vs the micro-well substrate.

earlier than from the flat surface, as pointed out earlier in the spreading ratio comparison depicted in Fig. 12.

The time variation of the non-dimensionalized drop kinetic energy is shown in Fig. 14. The impact speed is still 2.0 m/s, and the contact angle is 120°. After contacting the substrate, the kinetic energy quickly decreases to zero when the drop reaches the maximum liquid-substrate contact. As the drop starts to recede, the surface energy is converted to kinetic energy and the kinetic energy starts to increase. In Fig. 14, from $t^* = 1$ to $t^* = 2$ shows the gain in kinetic energy, which occurs during the recoiling phase after the event of the spreading. The drop on the micro-well has already detached at $t^* = 2.33$ and jumped-off with a higher kinetic energy and the kinetic energy for the drop on

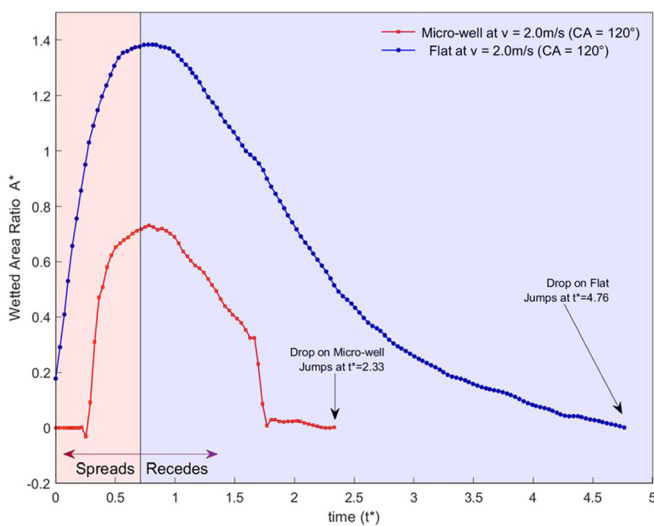


FIG. 13. Resulting wetted area ratio over time.

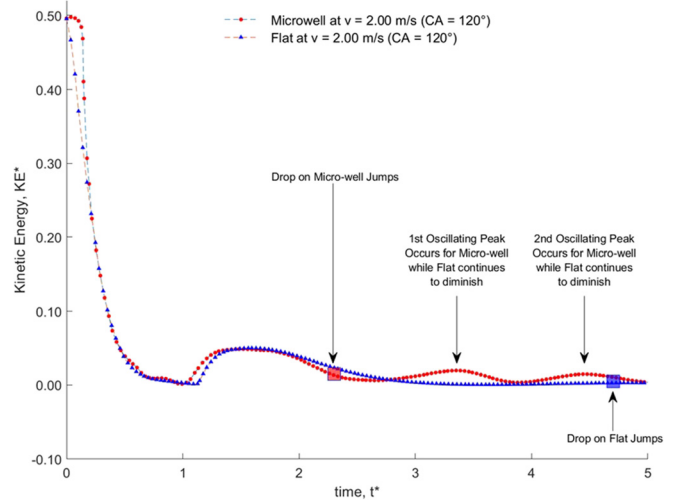


FIG. 14. Kinetic energy (KE^*) in the z-direction over time for drops impacting at various speeds at a contact angle of 120°.

the flat substrate continues to decrease, making it very difficult to detach from the surface. The kinetic energy of the drop on the micro-well, as presented by the red marker, while detached from the substrate, shows undulation with the first peak occurring from $t^* = 3$ to $t^* = 4$ and the second peak occurring from $t^* = 4$ to $t^* = 5$. In contrast, the kinetic energy for the drop on the flat substrate plateaus is close to zero and does not exhibit any oscillation, and the drop detaches from the substrate very later at $t^* = 4.76$. This comparison of the kinetic energy shows that the drop ejection is very slow for the flat substrate compared to the micro-well substrate, and it also becomes evident that larger wettability leads to the longer liquid–solid contact and diminishes kinetic energy for the drop with higher surface adhesion.

Effect of contact angle

We simulated the effect of the contact angle and the results at an impact speed of 0.75 m/s on the micro-well substrate. The time variation of the wetted area ratio, as defined in Eq. (18), is presented in Fig. 15 and the kinetic energy, as defined in Eq. (19), shown in Fig. 16. It is very apparent that the wetted area decreases with the increase in the contact angle: the smallest contact angle 120° case has the largest wetted area (drop-substrate contact area), and the largest contact angle 140° case has the smallest wetted area.

The contact angle influences the degree of adhesion, which in turn controls the outcome of the kinetic energy, as shown in Fig. 16. At $t^* = 1.25$, the drop reaches the maximum spreading extent, and therefore, the surface tension and the viscous forces overcame the liquid inertia, it starts to recede, and this is the instance where the surface energy begins to slowly convert into kinetic energy. The largest contact angle (140°) case has the smallest contact area, and less energy is used to detach from the surface which eventually results in a reserve of higher kinetic energy. On the contrary, the smallest contact angle case (120°) has the largest contact area with the substrate and, hence, has the lowest kinetic energy gain. Hence, liquid-substrate adhesion dictates the kinetic energy for the drop jumping behavior on the

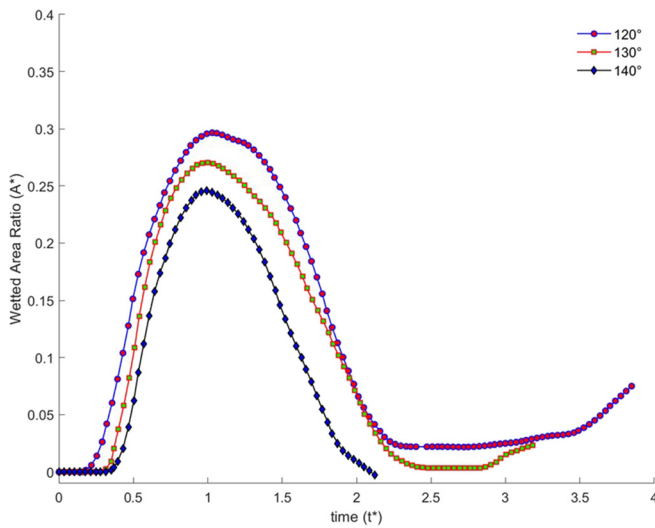


FIG. 15. Impact of the contact angle on the wetted area for drop impact on the micro-well substrate. The wetted area decreases with the increase in the contact angle.

micro-well substrate. With more drop-substrate contact, as in the case of 120°, results in less kinetic energy, and the drop fails to jump and starts to spread after the initial retraction and continues to oscillate while remaining in contact with the micro-well substrate. With a smaller liquid–solid contact in the case of 140°, the drop easily detaches and able to propel itself from the surface of the micro-well.

DROP JUMPING REGIME-MAP

Using the simulation results from different contact angles and impact speeds, we can quantitatively construct an impact velocity–contact angle jumping regime map, which entails the advantage of the

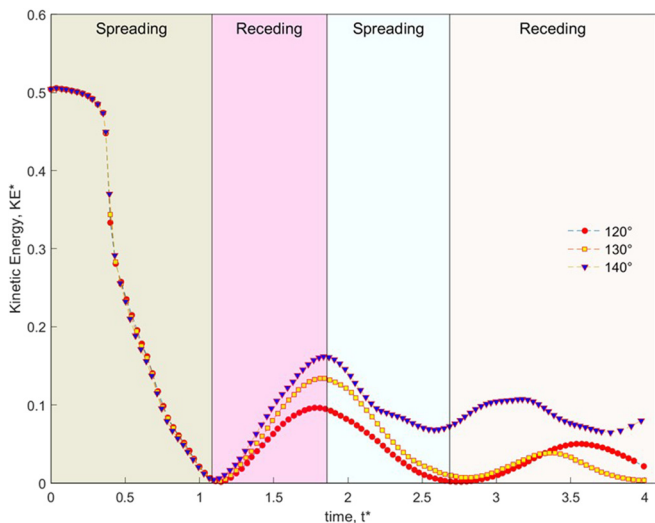


FIG. 16. Kinetic energy (KE*) in the z-direction over time for drops impacting at a speed of $v = 0.75$ m/s at contact angles of 120°, 130°, and 140°.

micro-well over a flat surface substrate and is presented in Fig. 17. It is evident that the micro-well jumping boundary is larger than the jumping boundary of the flat substrate.

We will further rationalize the ranges of the drop impacting and rebounding for all three contact angles presented in Fig. 17. For the contact angle of 120°, when the impact speed is lower than 1.4 m/s, the drop fails to detach from the flat surface and micro-well surface. When the impact speed is between 1.4 and 2.0 m/s, the drops can propel away from the micro-well substrate but not the flat substrate. When the impact speed is larger than 2.0 m/s, the drop can detach from both the flat and micro-well substrates. In the case of 130°, when the impact speed is between 0.7 and 0.85 m/s, the drop jumped from the micro-well substrate but not from the flat substrate. When the impact speed is smaller than 0.7 m/s, the kinetic energy cannot overcome the inter-surface adhesion forces in either case, and the drop does not detach from the substrates. At the contact angle of 140°, the jumping threshold on the micro-well substrate is more skewed than in the case of 130°. At a speed of 0.35–0.55 m/s, the drop can propel out of the micro-well surface but fail to detach from the flat substrate. At the impact speed of 0.55 m/s, the drop can jump off from both the micro-well and flat substrates.

Finally, to corroborate the structure of the regime map, we further illustrate by presenting three selected cases of impact speeds for two different contact angles at which the drop either (a) jumps from both substrates, (b) jumps off from the micro-well but not from the flat substrate, or (c) fails to propel from both substrates. Figure 18 presents the case of 130° contact angle, where impact speeds of (i) 1.0 m/s, (ii) 0.7 m/s, and (iii) 0.45 m/s are shown. Figure 19 shows the three speed cases of (i) 1.45 m/s, (ii) 1.15 m/s, and (iii) 0.35 m/s for the contact angle of 140°. At 130°, the drop in the case of 1.0 m/s jumps from both substrates, while at 0.7 m/s the drop jumps from the micro-well but fails on the flat substrate. At 140°, the drop rebounds on both the substrate types while the impacts speeds are $v = 1.45$ m/s and $v = 1.15$ m/s. For the slowest speed of 0.35 m/s, the drop slightly jumps

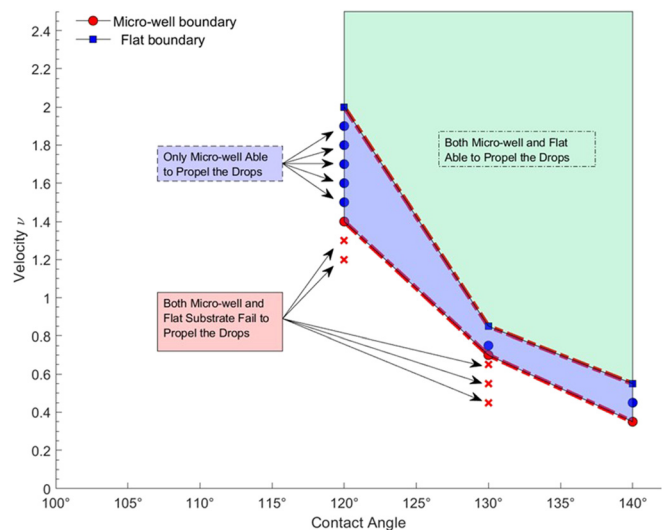


FIG. 17. Regime map showing the ability to propel drops on the micro-well and the flat substrate.

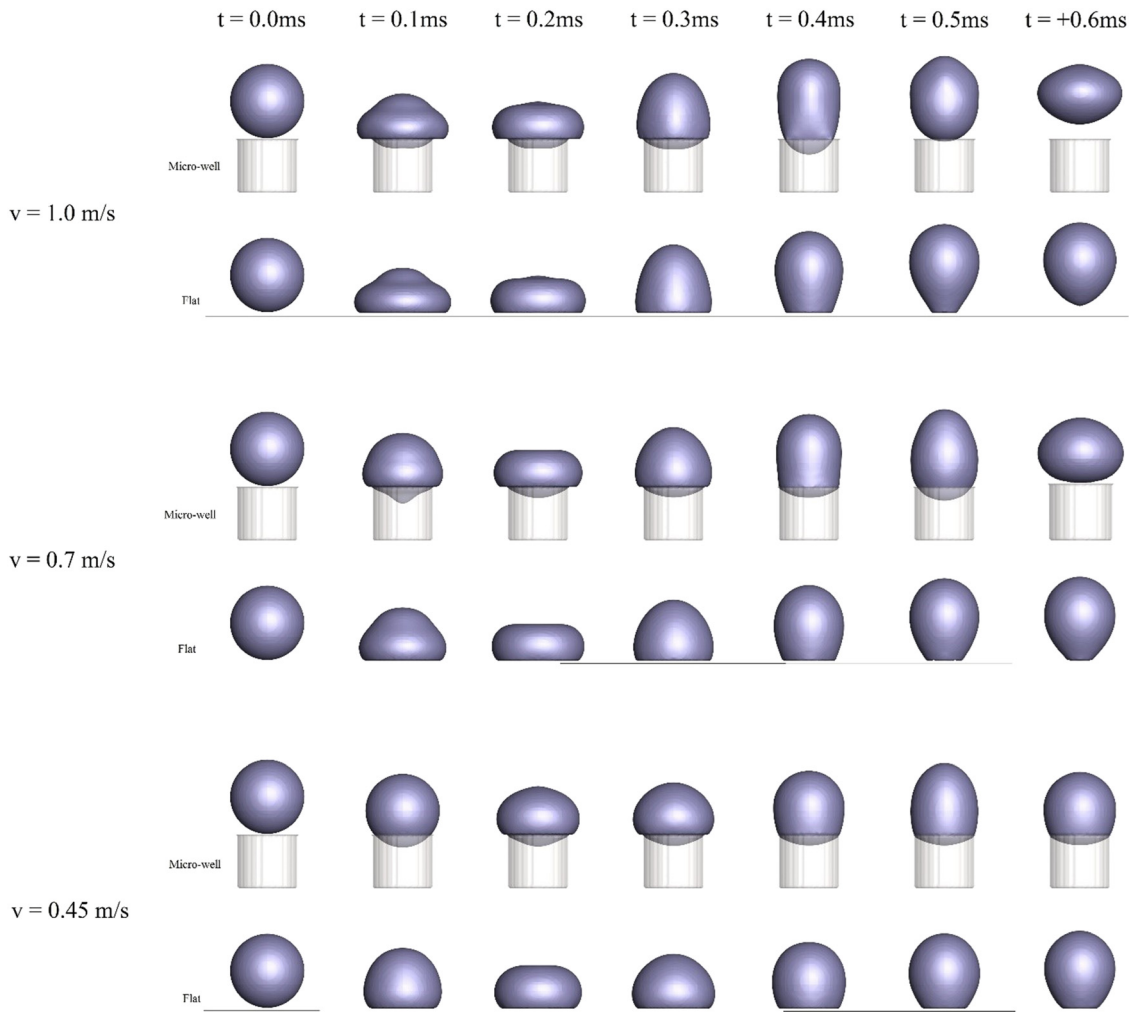


FIG. 18. Drop impact on the micro-well vs flat at a contact angle of 130° : different instances of jumping and non-jumping off the substrate.

from the micro-well but could not detach from the flat substrate. Thus, through our analysis, it is strongly evident that the micro-well has advantages in drop rebound capability, which is otherwise not possible on the flat smooth substrate over different impact speeds and different contact angles and wettability conditions.

Drop impact on a substrate with patterned micro-wells

Substrates designed in common experimental settings typically consist of several densely packed micro-structures to give the hydrophobicity nature to the surface that is intrinsically water repellent. As discussed earlier, air pockets within the micro-structure can prevent the drop from reaching the bottom of the substrate and, thus, reduces the solid–liquid contact area.^{49,62,89} Therefore, using the same concept of a large micro-well, we compare an array of the patterned micro-well case against a flat substrate for the contact angle of 120° . The drop impact speed is 1.9 m/s, and the size of the drop is $250\ \mu\text{m}$. The three-dimensional schematic for a drop on a substrate with an array of

micro-wells is shown in Fig. 20. The diameter of each of the single micro-well is $1.2\ \mu\text{m}$, and the distance (pitch) between one micro-well and the next is designed to be $2.725\ \mu\text{m}$.

As can be seen in Fig. 21, the drop on the micro-well easily detaches and jumps off from the micro-well array after $t = 0.45\ \text{ms}$, whereas the drop on the flat substrate fails to leave the substrate surface. Our finding confirms the widely accepted theoretical proposition of air entrapment behavior as presented forth by Quéré.^{26,90} Because of the Laplace pressure that exists between the liquid–solid interface of a much larger drop and much smaller roughness scale, the dry solid has lower surface energy, $\sigma_{\text{solid-vapor}}$, than the wet one, $\sigma_{\text{solid-liquid}}$, and therefore, if air traps inside the roughness with a given roughness factor of r , then it favors in lower surface energy.⁹¹ Quéré,^{26,90} using the reference to subsequent literatures,^{91–93} has expanded the equation form as shown below

$$(r - \phi_s)(\sigma_{\text{solid-liquid}} - \sigma_{\text{solid-vapor}}) > (1 - \phi_s)\sigma, \quad (21)$$

where ϕ_s is the fraction of the solid/liquid interface below the drop and results in the following thermodynamically stable (super)hydrophobic state:

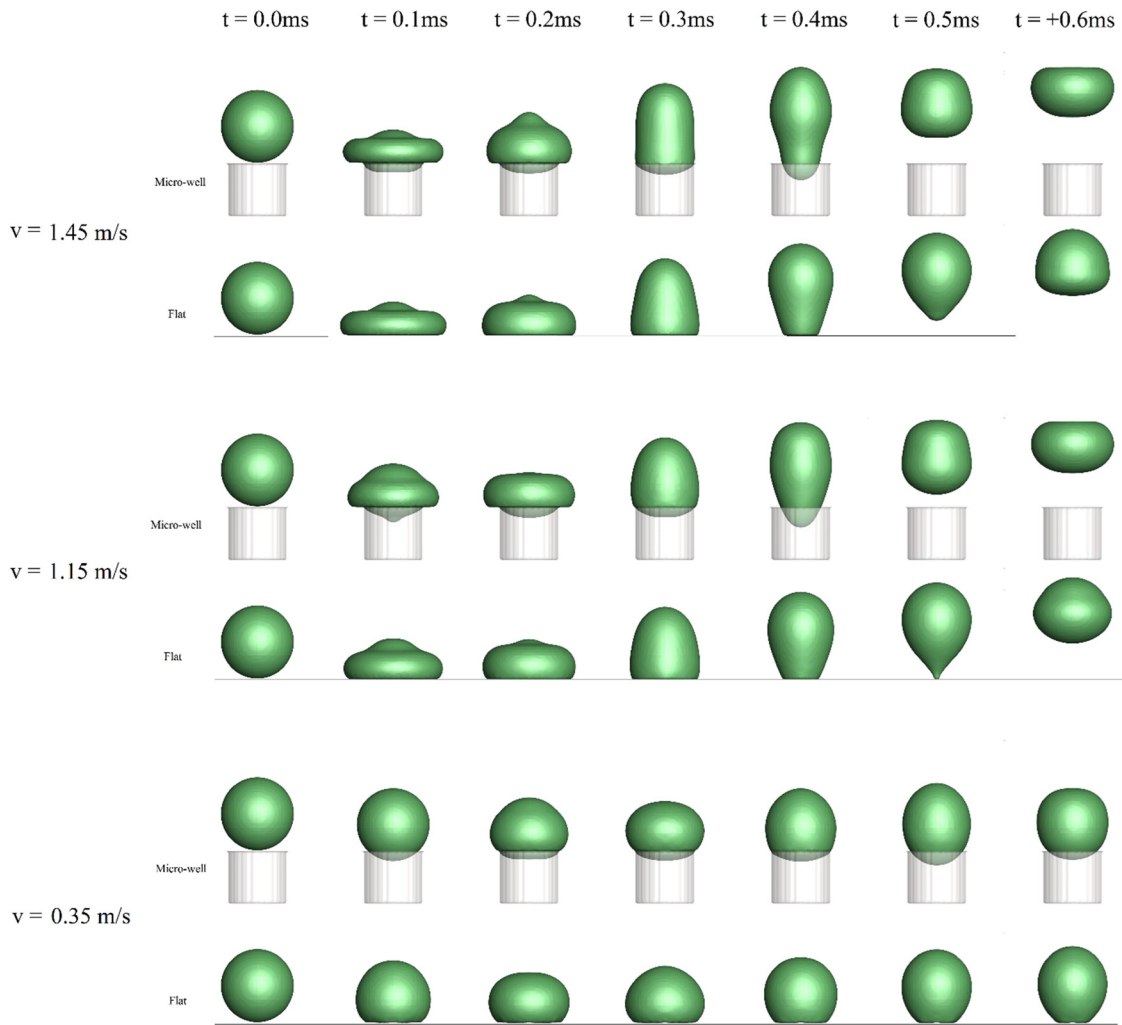


FIG. 19. Drop impact on the micro-well vs flat at a contact angle of 140° : different instances of jumping and non-jumping off the substrate.

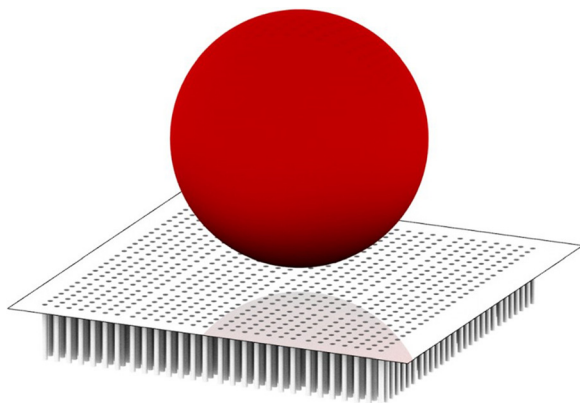


FIG. 20. Rendering of the setup of a drop impact on an array of the micro-well.

$$\cos \theta < \frac{\phi_s - 1}{r - \phi_s}. \tag{22}$$

A larger θ is inevitable with increased roughness r and, therefore, as presented in our simulation result, that increasing roughness to properly entrap air using an array of numerous micro-wells, increases hydrophobicity with water repellency nature of the solid on which the drop impacts. This is otherwise not possible with a smooth flat substrate, as shown in our simulation, and the water drop fails to detach from the surface and the non-wetting state is not achieved.

CONCLUSION

Using a sharp interface reconstruction method to track different phases, the non-wetting property of a micro-well is studied and compared with a flat solid surface. Our simulation predicted the impact, spreading, retraction, and possible jump off ability of drops impacting

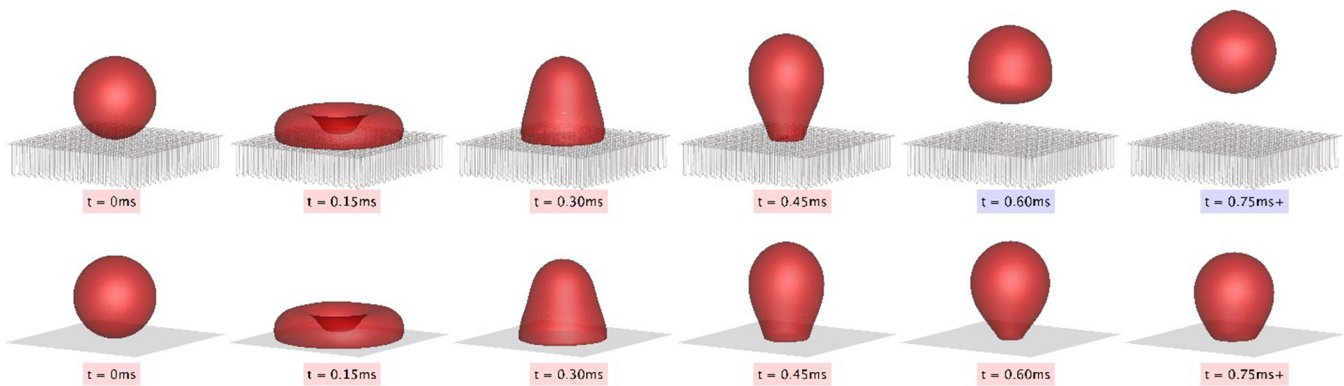


FIG. 21. Drop impact on an array of the micro-well (top) vs flat (bottom) surface: drop rebounds on the micro-well but fails on a flat substrate. The impact speed of 1.9 m/s at a contact angle of 120° .

on the micro-well and the flat substrate. The drop on the micro-well has smaller wetting area and significantly smaller spreading ratio. For a wide range of impact velocities, it was also found that the drop would be able to jump off on the micro-well substrate but otherwise fails to do so on the flat solid surface. The wetted area ratio analysis indicated the drop on the micro-well undergoes less solid–liquid adhesion. Consequently, the kinetic energy analysis found the micro-well substrate to be more water repelling than the flat substrate. A regime map has been constructed where the drop impact study of different velocities was extended over contact angles of 120° , 130° , and 140° . Finally, an array of the micro-well is constructed and contrasted with a flat smooth substrate, where the micro-well substrate shows excellent non-wettability by repelling a water drop which otherwise did not depart the surface of the flat substrate.

ACKNOWLEDGMENTS

This research was partially supported by a NSF grant (No. 1916114, program manager, Dr. William Olbricht).

AUTHOR DECLARATIONS

Conflict of Interest

The authors have no conflicts to disclose.

DATA AVAILABILITY

The data that support the findings of this study are available from the corresponding author upon reasonable request.

REFERENCES

- J. C. Bird, R. Dhiman, H.-M. Kwon, and K. K. Varanasi, “Reducing the contact time of a bouncing drop,” *Nature* **503**, 385 (2013).
- D. Bartolo, C. Josserand, and D. Bonn, “Retraction dynamics of aqueous drops upon impact on non-wetting surfaces,” *J. Fluid Mech.* **545**, 329 (2005).
- C. Clanet, C. Béguin, D. Richard, and D. Quéré, “Maximal deformation of an impacting drop,” *J. Fluid Mech.* **517**, 199 (2004).
- J. Fukai, Z. Zhao, D. Poulikakos, C. M. Megaridis, and O. Miyatake, “Modeling of the deformation of a liquid droplet impinging upon a flat surface,” *Phys. Fluids A* **5**, 2588 (1993).
- I. V. Roisman, R. Rioboo, and C. Tropea, “Normal impact of a liquid drop on a dry surface: Model for spreading and receding,” *Proc. R. Soc. London, Ser. A* **458**, 1411 (2002).
- F. Wang and T. Fang, “Retraction dynamics of water droplets after impacting upon solid surfaces from hydrophilic to superhydrophobic,” *Phys. Rev. Fluids* **5**, 033604 (2020).
- B. He, S. Yang, Z. Qin, B. Wen, and C. Zhang, “The roles of wettability and surface tension in droplet formation during inkjet printing,” *Sci. Rep.* **7**, 11841 (2017).
- C. D. Modak, A. Kumar, A. Tripathy, and P. Sen, “Drop impact printing,” *Nat. Commun.* **11**, 4327 (2020).
- M. Damak, M. N. Hyder, and K. K. Varanasi, “Enhancing droplet deposition through *in-situ* precipitation,” *Nat. Commun.* **7**, 12560 (2016).
- R. E. Gaskin, K. D. Steele, and W. A. Forster, “Characterising plant surfaces for spray adhesion and retention,” *N. Z. Plant Prot.* **58**, 179 (2005).
- G. J. Dorr, S. Wang, L. C. Mayo, S. W. McCue, W. A. Forster, J. Hanan, and X. He, “Impaction of spray droplets on leaves: Influence of formulation and leaf character on shatter, bounce and adhesion,” *Exp. Fluids* **56**, 143 (2015).
- J. D. Bernardin, C. J. Stebbins, and I. Mudawar, “Effects of surface roughness on water droplet impact history and heat transfer regimes,” *Int. J. Heat Mass Transfer* **40**, 73 (1996).
- L. Feng, M. Yang, X. Shi, Y. Liu, Y. Wang, and X. Qiang, “Copper-based superhydrophobic materials with long-term durability, stability, regenerability, and self-cleaning property,” *Colloids Surf., A* **508**, 39 (2016).
- H. Li, S. Yu, J. Hu, and X. Yin, “Modifier-free fabrication of durable superhydrophobic electrodeposited Cu-Zn coating on steel substrate with self-cleaning, anti-corrosion and anti-scaling properties,” *Appl. Surf. Sci.* **481**, 872 (2019).
- N. Wang, D. Xiong, Y. Deng, Y. Shi, and K. Wang, “Mechanically robust superhydrophobic steel surface with anti-icing, UV-durability, and corrosion resistance properties,” *ACS Appl. Mater. Interfaces* **7**, 6260 (2015).
- F. Hasan, K. A. H. Al Mahmud, M. I. Khan, S. Patil, B. H. Dennis, and A. Adnan, “Cavitation induced damage in soft biomaterials,” *Multiscale Sci. Eng.* **3**, 67 (2021).
- R. P. Selvam, L. Lin, and R. Ponnappan, “Direct simulation of spray cooling: Effect of vapor bubble growth and liquid droplet impact on heat transfer,” *Int. J. Heat Mass Transfer* **49**, 4265 (2006).
- J. D. Bernardin, C. J. Stebbins, and I. Mudawar, “Mapping of impact and heat transfer regimes of water drops impinging on a polished surface,” *Int. J. Heat Mass Transfer* **40**(2), 247–267 (1997).
- W. M. Healy, J. Hartley, and S. I. Abdel-Khalik, “On the validity of the adiabatic spreading assumption in droplet impact cooling,” *Int. J. Heat Mass Transfer* **44**, 3869 (2001).
- Y. Shen, H. Tao, S. Chen, L. Zhu, T. Wang, and J. Tao, “Icephobic/anti-icing potential of superhydrophobic Ti6Al4V surfaces with hierarchical textures,” *RSC Adv.* **5**, 1666 (2015).
- Y. Lai, Y. Tang, J. Huang, H. Wang, H. Li, D. Gong, X. Ji, J. Gong, C. Lin, L. Sun, and Z. Chen, “Multi-functional hybrid protonated titanate nanobelts with tunable wettability,” *Soft Matter* **7**, 6313 (2011).

- ²²S. Latthe, R. Sutar, A. Bhosale, S. Nagappan, C.-S. Ha, K. K. Sadasivuni, and R. Xing, "Recent developments in air-trapped superhydrophobic and liquid-infused slippery surfaces for anti-icing application," *Prog. Org. Coat.* **137**, 105373 (2019).
- ²³C. Neinhuis and W. J. Barthlott, "Characterization and distribution of water-repellent, self-cleaning plant surfaces," *Ann. Bot.* **79**, 667 (1997).
- ²⁴W. Barthlott and C. Neinhuis, "Purity of the sacred lotus, or escape from contamination in biological surfaces," *Planta* **202**, 1 (1997).
- ²⁵N. R. Bernardino, V. Blickle, and S. Dietrich, "Wetting of surfaces covered by elastic hairs," *Langmuir* **26**, 7233 (2010).
- ²⁶D. Quéré, "Non-sticking drops," *Rep. Prog. Phys.* **68**, 2495 (2005).
- ²⁷A. Mazloomi Moqaddam, S. S. Chikatamarla, and I. V. Karlin, "Drops bouncing off macro-textured superhydrophobic surfaces," *J. Fluid Mech.* **824**, 866 (2017).
- ²⁸K. Rykaczewski, T. Landin, M. L. Walker, J. H. J. Scott, and K. K. Varanasi, "Direct imaging of complex nano- to microscale interfaces involving solid, liquid, and gas phases," *ACS Nano* **6**, 9326 (2012).
- ²⁹C. Josserand and S. T. Thoroddsen, "Drop impact on a solid surface," *Annu. Rev. Fluid Mech.* **48**, 365 (2016).
- ³⁰K. Manoharan and S. Bhattacharya, "Superhydrophobic surfaces review: Functional application, fabrication techniques and limitations," *J. Micromanuf.* **2**, 59 (2019).
- ³¹M. Ma and R. M. Hill, "Superhydrophobic surfaces," *Curr. Opin. Colloid Interface Sci.* **11**, 193 (2006).
- ³²M. A. Nilsson, R. J. Daniello, and J. P. Rothstein, "A novel and inexpensive technique for creating superhydrophobic surfaces using Teflon and sandpaper," *J. Phys. D* **43**, 045301 (2010).
- ³³A. Ibekwe, Y. Tanino, and D. Pokrajac, "A low-cost, non-hazardous protocol for surface texturing of glass particles," *Tribol. Lett.* **67**, 115 (2019).
- ³⁴K. Kubiak, M. Wilson, T. Mathia, and P. J. Carval, "Wettability versus roughness of engineering surfaces," *Wear* **271**, 523 (2011).
- ³⁵L. F. de Moura and R. E. Hernández, "Effects of abrasive mineral, grit size and feed speed on the quality of sanded surfaces of sugar maple wood," *Wood Sci. Technol.* **40**, 517 (2006).
- ³⁶K. Regulagadda, S. Bakshi, and S. K. Das, "Morphology of drop impact on a superhydrophobic surface with macro-structures," *Phys. Fluids* **29**, 082104 (2017).
- ³⁷P. Chantelot, A. Mazloomi, A. Gauthier, S. S. Chikatamarla, C. Clanet, I. V. Karlin, and D. Quéré, "Water ring-bouncing on repellent singularities," *Soft Matter* **14**, 2227 (2018).
- ³⁸D. Khojasteh, A. Bordbar, R. Kamali, and M. Marengo, "Curvature effect on droplet impacting onto hydrophobic and superhydrophobic spheres," *Int. J. Comput. Fluid Dyn.* **31**, 310 (2017).
- ³⁹X. Liu, X. Zhang, and J. Min, "Droplet rebound and dripping during impact on small superhydrophobic spheres," *Phys. Fluids* **34**, 032118 (2022).
- ⁴⁰T. C. de Goede, A. M. Moqaddam, K. Limpens, S. Kooij, D. Derome, J. Carmeliet, N. Shahidzadeh, and D. Bonn, "Droplet impact of Newtonian fluids and blood on simple fabrics: Effect of fabric pore size and underlying substrate," *Phys. Fluids* **33**, 033308 (2021).
- ⁴¹Y. Xiao, C. Zhang, Q. Li, P. Yang, and D. He, "Study on micro-scale 3D numerical modeling and droplet deposition of plain weave fabric," *J. Mech. Sci. Technol.* **36**, 1739 (2022).
- ⁴²Y. Shen, S. Liu, C. Zhu, J. Tao, Z. Chen, H. Tao, L. Pan, G. Wang, and T. Wang, "Bouncing dynamics of impact droplets on the convex superhydrophobic surfaces," *Appl. Phys. Lett.* **110**, 221601 (2017).
- ⁴³X. Liu, Y. Zhao, S. Chen, S. Shen, and X. Zhao, "Numerical research on the dynamic characteristics of a droplet impacting a hydrophobic tube," *Phys. Fluids* **29**, 062105 (2017).
- ⁴⁴Y. Liu, M. Andrew, J. Li, J. M. Yeomans, and Z. Wang, "Symmetry breaking in drop bouncing on curved surfaces," *Nat. Commun.* **6**, 10034 (2015).
- ⁴⁵L. Moevius, Y. Liu, Z. Wang, and J. M. Yeomans, "Pancake bouncing: Simulations and theory and experimental verification," *Langmuir* **30**, 13021 (2014).
- ⁴⁶D. Bartolo, F. Bouamrine, É. Verneuil, A. Buguin, P. Silberzan, and S. Moulinet, "Bouncing or sticky droplets: Impalement transitions on superhydrophobic micropatterned surfaces," *Europhys. Lett.* **74**, 299 (2006).
- ⁴⁷D. Hee Kwon and S. Joon Lee, "Impact and wetting behaviors of impinging microdroplets on superhydrophobic textured surfaces," *Appl. Phys. Lett.* **100**, 171601 (2012).
- ⁴⁸M. Reyssat, A. Pépin, F. Marty, Y. Chen, and D. Quéré, "Bouncing transitions on microtextured materials," *Europhys. Lett.* **74**, 306 (2006).
- ⁴⁹W. Fang, H.-Y. Guo, B. Li, Q. Li, and X.-Q. Feng, "Revisiting the critical condition for the Cassie–Wenzel transition on micropillar-structured surfaces," *Langmuir* **34**, 3838 (2018).
- ⁵⁰A. Giacomello, M. Chinappi, S. Meloni, and C. M. Casciola, "Metastable wetting on superhydrophobic surfaces: Continuum and atomistic views of the Cassie–Baxter–Wenzel transition," *Phys. Rev. Lett.* **109**, 226102 (2012).
- ⁵¹X. He, B.-X. Zhang, S.-L. Wang, Y.-F. Wang, Y.-R. Yang, X.-D. Wang, and D.-J. Lee, "The Cassie-to-Wenzel wetting transition of water films on textured surfaces with different topologies," *Phys. Fluids* **33**, 112006 (2021).
- ⁵²C. Lee, Y. Nam, H. Lastakowski, J. I. Hur, S. Shin, A.-L. Biance, C. Pirat, C. J. Kim, and C. Ybert, "Two types of Cassie-to-Wenzel wetting transitions on superhydrophobic surfaces during drop impact," *Soft Matter* **11**, 4592 (2015).
- ⁵³C. Guo, L. Liu, J. Sun, C. Liu, and S. Liu, "Splashing behavior of impacting droplets on grooved superhydrophobic surfaces," *Phys. Fluids* **34**, 052105 (2022).
- ⁵⁴F. Yeganehdoust, R. Attarzadeh, A. Dolatabadi, and I. Karimfazli, "A comparison of bioinspired slippery and superhydrophobic surfaces: Micro-droplet impact," *Phys. Fluids* **33**, 022105 (2021).
- ⁵⁵O. Bliznyuk, E. Vereshchagina, E. S. Kooij, and B. Poelsema, "Scaling of anisotropic droplet shapes on chemically stripe-patterned surfaces," *Phys. Rev. E* **79**, 041601 (2009).
- ⁵⁶S. Kulinich and M. Farzaneh, "How wetting hysteresis influences ice adhesion strength on superhydrophobic surfaces," *Langmuir* **25**, 8854 (2009).
- ⁵⁷C. Antonini, F. Villa, and M. Marengo, "Oblique impacts of water drops onto hydrophobic and superhydrophobic surfaces: Outcomes, timing, and rebound maps," *Exp. Fluids* **55**, 1713 (2014).
- ⁵⁸A. Lafuma and D. Quéré, "Superhydrophobic states," *Nat. Mater.* **2**, 457 (2003).
- ⁵⁹C. Dorrer and J. J. Rühle, "Some thoughts on superhydrophobic wetting," *Soft Matter* **5**, 51 (2009).
- ⁶⁰A. J. Meuler, G. H. McKinley, and R. E. Cohen, "Exploiting topographical texture to impart icephobicity," *ACS Nano* **4**, 7048 (2010).
- ⁶¹X. Yao, Y. Song, and L. Jiang, "Applications of bio-inspired special wettable surfaces," *Adv. Mater.* **23**, 719 (2011).
- ⁶²P. Papadopoulos, L. Mammen, X. Deng, D. Vollmer, and H.-J. Butt, "How superhydrophobicity breaks down," *Proc. Natl. Acad. Sci.* **110**, 3254 (2013).
- ⁶³D. Khojasteh, M. Kazerooni, S. Salarian, and R. Kamali, "Droplet impact on superhydrophobic surfaces: A review of recent developments," *J. Ind. Eng. Chem.* **42**, 1 (2016).
- ⁶⁴A. L. Yarin, "Drop impact dynamics: Splashing, spreading, receding, bouncing...", *Annu. Rev. Fluid Mech.* **38**, 159 (2006).
- ⁶⁵D. Richard and D. Quéré, "Bouncing water drops," *Europhys. Lett.* **50**, 769 (2000).
- ⁶⁶R. B. Bird, "Transport phenomena," *Appl. Mech. Rev.* **55**, R1 (2002).
- ⁶⁷X. Li, X. Ma, and Z. Lan, "Dynamic behavior of the water droplet impact on a textured hydrophobic/superhydrophobic surface: The effect of the remaining liquid film arising on the pillars' tops on the contact time," *Langmuir* **26**, 4831 (2010).
- ⁶⁸M. Reyssat, D. Richard, C. Clanet, and D. Quéré, "Dynamical superhydrophobicity," *Faraday Discuss.* **146**, 19 (2010).
- ⁶⁹Y. Qian and L.-Z. Zhang, "Numerical and analytical study of the impinging and bouncing phenomena of droplets on superhydrophobic surfaces with microtextured structures," *Langmuir* **30**, 11640 (2014).
- ⁷⁰X. Huang, K.-T. Wan, and M. E. Taslim, "Axisymmetric rim instability of water droplet impact on a super-hydrophobic surface," *Phys. Fluids* **30**, 094101 (2018).
- ⁷¹G. Castanet, W. Chaze, O. Caballina, R. Collignon, and F. Lemoine, "Transient evolution of the heat transfer and the vapor film thickness at the drop impact in the regime of film boiling," *Phys. Fluids* **30**, 122109 (2018).

- ⁷²R. Rioboo, M. Marengo, and C. Tropea, "Outcomes from a drop impact on solid surfaces," *Atomization Sprays* **11**, 12 (2001).
- ⁷³V. Dyadechko and M. Shashkov, "Reconstruction of multi-material interfaces from moment data," *J. Comput. Phys.* **227**, 5361 (2008).
- ⁷⁴M. Jemison, M. Sussman, and M. Arienti, "Compressible, multiphase semi-implicit method with moment of fluid interface representation," *J. Comput. Phys.* **279**, 182 (2014).
- ⁷⁵M. Jemison, M. Sussman, and M. Shashkov, "Filament capturing with the multimaterial moment-of-fluid method," *J. Comput. Phys.* **285**, 149 (2015).
- ⁷⁶Y. Liu, M. Sussman, Y. Lian, M. Y. Hussaini, M. Vahab, and K. Shoele, "A novel supermesh method for computing solutions to the multi-material Stefan problem with complex deforming interfaces and microstructure," *J. Sci. Comput.* **91**, 19 (2022).
- ⁷⁷G. Li, Y. Lian, Y. Guo, M. Jemison, M. Sussman, T. Helms, and M. Arienti, "Incompressible multiphase flow and encapsulation simulations using the moment-of-fluid method," *Int. J. Numer. Methods Fluids* **79**, 456 (2015).
- ⁷⁸H. T. Ahn and M. Shashkov, "Multi-material interface reconstruction on generalized polyhedral meshes," *J. Comput. Phys.* **226**, 2096 (2007).
- ⁷⁹H. T. Ahn and M. Shashkov, "Adaptive moment-of-fluid method," *J. Comput. Phys.* **228**, 2792 (2009).
- ⁸⁰M. Cutforth, P. T. Barton, and N. Nikiforakis, "An efficient moment-of-fluid interface tracking method," *Comput. Fluids* **224**, 104964 (2021).
- ⁸¹V. Dyadechko and M. Shashkov, "Moment-of-fluid interface reconstruction," Los Alamos Report No. LA-UR-05-7571 (Los Alamos National Laboratory, 2005).
- ⁸²M. Jemison, E. Loch, M. Sussman, M. Shashkov, M. Arienti, M. Ohta, and Y. Wang, "A coupled level set-moment of fluid method for incompressible two-phase flows," *J. Sci. Comput.* **54**, 454 (2013).
- ⁸³A. A. Mukundan, T. Ménard, J. C. B. de Motta, and A. Berlemont, "A 3D moment of fluid method for simulating complex turbulent multiphase flows," *Comput. Fluids* **198**, 104364 (2020).
- ⁸⁴H. Y. Kim and J. H. Chun, "The recoiling of liquid droplets upon collision with solid surfaces," *Phys. Fluids* **13**, 643 (2001).
- ⁸⁵T.-S. Jiang, O. H. Soo-Gun, and J. C. Slattery, "Correlation for dynamic contact angle," *J. Colloid Interface Sci.* **69**, 74 (1979).
- ⁸⁶X. Chen, J. Lu, and G. Tryggvason, "Numerical simulation of self-propelled non-equal sized droplets," *Phys. Fluids* **31**, 052107 (2019).
- ⁸⁷Y. Chen, A. Islam, M. Sussman, and Y. Lian, "Numerical investigation of surface curvature effect on the self-propelled capability of coalesced drops," *Phys. Fluids* **32**, 122117 (2020).
- ⁸⁸Y. A. Cengel and J. M. Cimbala, "Properties of fluids," *Fluid Mechanics: Fundamentals Applications* (McGraw Hill, 2014), Vol. 37.
- ⁸⁹Y. Shen, X. Xie, J. Tao, H. Chen, Z. Cai, S. Liu, and J. Jiang, "Mechanical equilibrium dynamics controlling wetting state transition at low-temperature superhydrophobic array-microstructure surfaces," *Coatings* **11**, 522 (2021).
- ⁹⁰D. Quéré, "Wetting and roughness," *Annu. Rev. Mater. Res.* **38**, 71 (2008).
- ⁹¹J. Bico, U. Thiele, and D. Quéré, "Wetting of textured surfaces," *Colloids Surf., A* **206**, 41 (2002).
- ⁹²G. Alberti and A. DeSimone, "Wetting of rough surfaces: A homogenization approach," *Proc. R Soc. A* **461**, 79 (2005).
- ⁹³N. A. Patankar, "On the modeling of hydrophobic contact angles on rough surfaces," *Langmuir* **19**, 1249 (2003).